NASA Technical Memorandum 81547

ANISOTROPIC TRIBOLOGICAL PROPERTIES OF SILICON CARBIDE

Kazuhisa Miyoshi and Donald H. Buckley
Lewis Research Center
Cleveland, Ohio

Prepared for the
International Conference on Wear of Materials
cosponsored by the American Society of Mechanical Engineers and Japan Society of Lubrication Engineers
San Francisco, California, March 30-April 1, 1981

NASA

ANISOTROPIC TRIBOLOGICAL PROPERTIES OF SILICON CARBIDE

by Kazuhisa Miyoshi and Donald H. Buckley

National Aeronautics and Space Administration
Lewis Research Center
Cleveland, Ohio 44135

ABSTRACT

The anisotropic friction, deformation and fracture behavior of single-crystal silicon carbide surfaces were investigated in two categories. The first, is that in which friction and wear of silicon carbide arises primarily from adhesion between sliding solid surfaces in contact, and second is where friction and wear of silicon carbide occur as a result of the surface sliding against a hard particle. The categories are called adhesive and abrasive wear processes, respectively. In the adhesive wear process, the adhesion, friction and wear of silicon carbide are markedly dependent on crystallographic orientation. The force to reestablish the shearing fracture of adhesive bond at the interface between silicon carbide and metal is the lowest in the preferred orientation of silicon carbide slip system. The fracturing of silicon carbide occurs near the adhesive bond to metal and it is due to primary cleavages of both prismatic $\{10\bar{1}0\}$ and basal $\{0001\}$ planes. In the abrasion process of silicon carbide the $\langle 10\bar{1}0\rangle$ direction on the basal plane exhibits the lowest coefficient of friction and the greatest resistance to abrasion for silicon carbide. The anisotropic friction and plastic deformation are primarily controlled by the slip system $\{10\bar{1}0\}\langle 11\bar{2}0\rangle$. The anisotropic fracture in the abrasion process is due to primary cleavages of $\{0001\}$, $\{10\bar{1}0\}$ and $\{11\bar{2}0\}$ planes.

INTRODUCTION

The high strength, excellent oxidation, and creep resistance as well as semiconducting properties of silicon carbide makes it an extremely important material for high temperature mechanical and electronic applications in hostile environments. Examples of its application include use as stable high-temperature semiconductors, gas turbine blades, turbine ceramic seals, and as an abrasive in grinding (1,2).

Silicon carbide has been studied in a number of fields including material science, solid state physics, metallurgy, etc. A wide variety of its properties have been investigated including ultrapurification, growth, crystal structure, new device concepts, physical, chemical, structural, optical, and electronic properties (1,2). Despite the wide scope of property studies, there is a lack of fundamental understanding relative to the surface science of silicon carbide, that is, its surface chemistry and physics. The present authors have conducted experimental studies to gain a better understanding of the surface chemistry and physics of single-cyrstal silicon carbide and its tribological properties under a variety of exacting environmental conditions (3-5).

Properties such as atomic density, spacing of atomic planes, surface energy, modulus of elasticity, slip systems, influence of imperfections, deformation, fracture and hardness have all been related to crystal orientation.

Anisotropic friction and deformation studies have been made by many investigators with a variety of salt structures (MgO, LiF, NaCl, etc.) as well as for some of the wear-resistant materials such as sapphire, diamond, and ferric oxide (6-16).

Although considerable effort has been put forth in determining the anisotropic friction behavior of single crystals on a variety of crystallographic planes and directions, the anisotropic friction and wear arise primarily from nonadhesive processes, such as abrasion. Very few studies of the anisotropic nature of friction and wear have been conducted from the consideration of adhesion between the sliding surfaces.

The objective of this paper is to describe the effects of crystallographic orientation on the tribological properties, that is, the friction and wear behavior of single-crystal silicon carbide surfaces in contact with various solids.

For simplicity of discussion, the tribological properties and the effect of crystallographic orientation on them are divided into two categories. The first is that in which the friction and wear of the silicon carbide airses primarily from adhesion between solid surfaces in sliding contact, and the second is where the friction and wear of silicon carbide occur as a result of the surface sliding against a hard particle. The two categories are called the adhesive and the abrasive wear processes, respectively. Two types of sliding friction experiments were conducted with the single-crystal silicon carbide. The first is conducted with silicon carbide in contact with metals or silicon carbide in vacuum, and the second is conducted with silicon carbide in contact with a diamond rider in mineral oil or in argon at atmospheric pressure. The vacuum environment is used in order to maximize the adhesion effect, while the oil and argon atmosphere is used to minimize the adhesion effect.

MATERIALS

The α single-crystal silicon carbide used in these experiments was a 99.9 percent pure compound of silicon and carbon. The unit cell of α-SiC is hexagonal with $a = 3.0817$ Å, $C = 15.1183$ Å, and has 21 molecules per unit cell (17,18). The method of growth is carbon arc.

Specimens were within $\pm 2^{\circ}$ of the low index $\{0001\}$ plane, and $\pm 3^{\circ}$ of $\{10\bar{1}0\}$ and $\{11\bar{2}0\}$ planes. The silicon carbide samples were in the form of flat platelets. The roughness of the mirror-polished silicon carbide surfaces measured by surface profilemeter was 0.3 micrometer for the maximum height of irregularities.

The metals (W, Fe, Rh, Ni, Ti, Co, Cu and Al) were all polycrystalline. The titanium was 99.97 percent pure, and the copper was 99.999 percent pure. All other metals were 99.99 percent pure. The radius of metal pin (rider) specimen was 0.79 mm.

The diamonds were commercially purchased. Diamond, the hardest known material, indents silicon carbide without itself suffering permanent deformation. It is elastic constants are also very high. The Young's modulus of silicon carbide is about 4.5×10^5 pascals, while that of diamond lies between 7×10^5 and 10×10^5 pascals (19,20).

APPARATUS

Two apparatuses were used in this investigation. One was a vacuum system capable of measuring adhesion, load, and friction. The apparatus also contained tools

for surface analysis, and an Auger electron spectroscopy (AES). The mechanism used for measuring adhesion, load, and friction is shown schematically in Fig. 1(a). A gimbal-mounted beam is projected into the vacuum system. The beam contains two flats machined normal to each other with strain gages mounted thereon. The end of the rod contains the metal or silicon carbide rider. As the beam is moved normal to the flat specimen, a load is applied that is measured by the strain gage. The vertical sliding motion of the rider along the flat surface is accomplished through a motorized gimbal assembly. Under an applied load, the friction force is sensed by the strain gage normal to that used to measure load. Multiple wear tracks could be generated on the flat specimen surface by translational motion of the beam containing the rider. This feature was used to examine the coefficient of friction at various loads. Rider sliding was in the vertical direction, as shown in Fig. 1(a). The vacuum apparatus in which the components of Fig. 1(a) were contained also had an AES. The electron beam from AES could be focused on any flat site desired. The second apparatus was a system capable of measuring friction in oil. The mechanism for measuring friction is shown schematically in Fig. 1(b). The beam contains one flat machined normal to the direction of friction application. The end of the rod contains the diamond rider. The load is applied by placing deadweights on a pan that sits on top of the rod. Under an applied load the friction force is sensed by a strain gage.

EXPERIMENTAL PROCEDURE

Adhesive wear. The flat and rider specimens were polished with a 3 micrometer diamond powder and then a 1 micrometer aluminum oxide powder. The radius of rider was 0.79 millimeter. Both specimens were rinsed with 200-proof ethyl alcohol.

For the experiments in vacuum the specimens were placed in the vacuum chamber and the system was evacuated and subsequently baked out to achieve a pressure of 1.3×10^{-8} N/m^2 (10^{-10} Torr). Two specimen cleaning procedures were used for silicon carbide in vacuum: (1) argon sputter cleaning, and (2) heating to 800° C. In the first procedure, argon gas was bled back into the vacuum chamber to a pressure of 1.3 pascal. A 1000-volt, direct-current potential was applied and the specimens (both flat and rider) were argon sputter bombarded for 30 minutes. After 1 hour the vacuum chamber was reevacuated and Auger spectra of the flat surface were obtained to determine the degree of surface cleanliness.

The second procedure examined included a resistance heating in situ to a temperature of 800° C at a pressure of 10^{-8} pascal for an hour and subsequent cooling to room temperature with the crystal in the as-received state after having been baked out in the vacuum chamber. The temperature of the silicon carbide surface was measured with a conventional thermocouple in direct contact with the surface of the silicon carbide specimen. The rider specimen was argon sputter cleaned. When the flat and rider surfaces were clean, friction experiments were conducted.

Loads of 5 to 50 grams were applied to the rider-flat contact by deflecting the beam of Fig. 1(a). Both load and friction force were continuously monitored during a friction experiment. Sliding velocity was 3 mm/min, with a total sliding distance of 3 millimeters. All friction experiments in vacuum were conducted with the system reevacuated to a pressure of 10^{-8} N/m^2.

Abrasive wear. The diamond riders were conical. The apical angle of conical rider was 117° ±1° and the radius of curvature at the apex was less than 5 micrometer. The riders were polished with 1 micrometer aluminum oxide powder before each friction experiment. The silicon carbide was polished with diamond and aluminum powder, as above mentioned. Both silicon carbide and diamond surfaces were rinsed with water and 200-proof ethyl alcohol before use. The friction experiments were single-pass, with a total sliding distance of 2 mm, at a sliding velocity of 3 mm/min in pure mineral oil (21) or in argon at atmospheric pressure.

RESULTS AND DISCUSSION

Adhesive Wear and Friction

Cleanliness of silicon carbide surfaces. An AES spectrum of the single-crystal silicon carbide surfaces obtained before sputter or heat cleaning, but after polishing and bake out, revealed an oxygen peak in addition to the silicon and carbon. The oxygen peak, and the chemically shifted silicon peaks at 78 and 89 electron volts indicated a layer of SiO_2 on the silicon carbide surfaces as well as a simple, adsorbed film of oxygen. The carbon peak was similar to that obtained for amorphous-carbon (22). Thus, the spectrum indicated a carbon contaminant on the silicon carbide surface as well as the SiO_2 layer.

The AES spectrum taken after the silicon carbide surface had been argon-sputter cleaned clearly reveals the silicon at 91 or 92 eV and carbon peaks at 272 eV, as shown in Fig. 2(a). The carbon peak is of the carbide type, which is characterized by three peak labelled A_0 to A_2 in Fig. 2(a). A small argon peak is evident in the spectrum, but the oxygen peak is negligible.

The spectrum of the surface preheated to 800° C is almost the same as that obtained for an argon sputter cleaned surface, as indicated by the data in Fig. 2. The spectrum of this surface reveals that main silicon peak appears at 88 eV, and the carbon peak of the carbide type is at 271 eV. No argon and oxygen peaks, however, are seen in the spectrum. Friction experiments were conducted in vacuum with surfaces cleaned in the manner just described.

Wear. Sliding friction experiments were conducted with silicon carbide (0001) surface in contact with various metals (W, Fe, Rh, Ni, Ti, Co, Cu, and Al), and the silicon carbide itself. All the silicon carbide surfaces contacted by the metals investigated were found to have transferred metals on the silicon carbide surface even with a single pass of a metal rider. Typical examples of metal transfer are shown in Fig. 3. The coefficient of friction for silicon carbide in contact with various metals was related to the relative chemical activity of the metals. The more active the metal (e.g., aluminum and titanium), the higher the coefficient of friction (3). The chemical activity of the metal and its shear modulus also play important roles in metal-transfer and wear. The more active the metal, and the less resistance it has to shear, the greater the transfer to silicon carbide (3).

The coefficient of friction for silicon carbide in sliding contact with silicon carbide itself is almost the same as those for silicon carbide in contact with the chemically active metals titanium and aluminum. The coefficient of friction is approximately 0.6. When repeated passes were made of the metal riders over the same single-crystal silicon carbide surface, the coefficient of friction generally decreased with the number of passes to an equilibrium value which depended on the nature of transfer of the metals. In contrast, when repeated passes were made with the silicon carbide rider on silicon carbide, the coefficient of friction was generally constant at 0.6.

The sliding of a metal or silicon carbide rider on a silicon carbide flat (0001) surfaces results in cracks along cleavage planes of $\{10\bar{1}0\}$ orientation. Figure 3 shows scanning electron micrographs of the wear tracks, generated by 10 passes of rhodium and titanium riders, on the silicon carbide (0001) surface along

the $\langle 10\bar{1}0 \rangle$ direction. The cracks, which are observed in the wear tracks, primarily propagate along cleavage planes of the $\{10\bar{1}0\}$ orientation. In Fig. 3(a), a hexagon-shaped light area is the beginning of wear track, and there is a large crack where cracks primarily along the $\{10\bar{1}0\}$ planes were generated, propagated, and then intersected during loading and sliding of the rhodium rider over the silicon carbide surface. It is anticipated from Fig. 3(a) that subsurface-cleavage cracking of the {0001} planes, which are parallel to the sliding surface, also occurs. Figure 3(b) reveals a hexagon-shaped pit and a copious amount of thin titanium film around the pit. The hexagon-shaped fracturing is primarily due to cleavage-cracking along $\{10\bar{1}0\}$ planes and subsurface-cleavage-cracking along the {0001} plane. The very smooth surface at the bottom of hexagon-pit is due to cleavage of the {0001} planes.

Figure 4 illustrates detailed examination of silicon carbide wear debris produced by 10-pass sliding of aluminum riders on the silicon carbide surface. The scanning electron micrographs already reveal evidence of multiangular wear debris particles of silicon carbide with transferred aluminum wear debris on the silicon carbide wear track. Such multiangular wear debris particles have crystallographically oriented sharp edges. They had shapes which were nearly hexagon, rhombus, parallelogram, or square (23). These shapes may be related to surface and subsurface cleavage of $\{10\bar{1}0\}$, $\{11\bar{2}0\}$, and {0001} planes.

Similar hexagon-shaped pit and multiangular wear debris, having crystallographically oriented sharp edges, were also observed with single-crystal silicon carbide in contact with itself. Figure 5 clearly reveals the gross hexagonal shaped pits on the wear scar of silicon carbide rider and a nearly full hexagon-shape and flat wear particle. The wear debris was observed to transfer to the flat specimen of silicon carbide. Thus, the crystallographically oriented cracking and fracturing of silicon carbide occurred as a result of sliding of the metal or the silicon carbide rider.

Friction. Friction experiments were conducted with the iron rider sliding on a silicon carbide (0001) surface, which was cleaned by heating to a temperature 800° C in vacuum. The frictional properties of the silicon carbide (0001) surface in contact with iron at temperatures up to 800° C is indicated in the data of Fig. 6. Auger analysis indicated that the reheated surface after the cleaning processes was the same as that of cleaned surface. The coefficient of friction generally increases with increasing temperature from about 0.5 in the $\langle 10\bar{1}0 \rangle$ sliding direction and 0.4 in the $\langle 11\bar{2}0 \rangle$ sliding direction at room temperature to 0.75 and 0.63 at about 800° C, respectively. Although the coefficient of friction remains low below 300° C, it increases rapidly with increasing temperature in the range of 300° to 600° C. There is then, however, little further increase in friction above 600° C.

The rapid increase in friction at temperatures of 300° to 600° C can be related to an increase in the adhesion resulting from recrystallization of iron. Iron normally has a recrystallization temperature of 200° to 300° C. The experiments herein were started with a deformed surface of polycrystalline iron. At temperatures of 300° to 600° C, recrystallization will occur for iron in contact with the silicon carbide. Recrystallized-annealed iron surfaces are less resistant to deformation and adhesion than are deformed surfaces. The general increases in friction at elevated temperatures are then due to the increased adhesion and plastic flow in the area of contact.

The data of Fig. 6 indicate that the friction behavior of silicon carbide in contact with iron is highly anisotropic over the entire temperature range of room temperature to 800° C. With silicon carbide several slip systems have been observed in α-silicon carbide, including the {0001} $\langle 11\bar{2}0 \rangle$, $\{3\bar{3}01\}$ $\langle 11\bar{2}0 \rangle$ and $\{10\bar{1}0\}$ $\langle 11\bar{2}0 \rangle$ (24,25). The preferred crystallographic slip direction or the direction of shear for the basal {0001} plane is the $\langle 11\bar{2}0 \rangle$ direction. Examination of the coefficient of friction on the basal plane indicates that the coefficient of friction is lower in the $\langle 11\bar{2}0 \rangle$ direction than it was in the $\langle 10\bar{1}0 \rangle$ direction. The coefficient of friction reflects the force required to shear at the interface with the basal planes of the silicon carbide parallel to the interface. The results presented in Fig. 6 indicate that the force to resist the shearing fracture of the adhesion bond at the interface is lower in the preferred crystallographic direction than it is in the $\langle 10\bar{1}0 \rangle$ direction.

Silicon carbide {0001} surfaces, which were argon sputter cleaned or were heat cleaned in situ, revealed no significant difference in coefficient of friction. The frictional anisotropy is also similar, that is, the coefficient of friction is lower in the $\langle 11\bar{2}0 \rangle$ direction than it was in the $\langle 10\bar{1}0 \rangle$ direction.

Abrasive Wear and Friction

Hardness. As hardness is a conventionally used parameter for indicating abrasion resistance, it is useful to attempt an examination of hardness anisotropy of silicon carbide. Figure 7 represents a back reflection Laue photograph and the results of Knoop hardness experiments made on the {0001} plane of silicon carbide. Specimens were less than ±2° of the low index {0001} plane. The Knoop hardness is presented as a function of orientation with the long axis of the indenter in the $\langle 10\bar{1}0 \rangle$ direction at 10° intervals. The hardness decreases smoothly to a minimum value of about 2670 located near 30° from the $\langle 10\bar{1}0 \rangle$ direction. Figure 7 indicates that the $\langle 10\bar{1}0 \rangle$ direction is the maximum hardness direction and the value of hardness is about 2830. The hardness results are very consistent with those of Shaffer and Adewoye (26,27).

Wear. Sliding friction experiments were conducted with a conical diamond rider in contact with flat silicon carbide {0001}, $\{10\bar{1}0\}$, and $\{11\bar{2}0\}$ surfaces in mineral oil at atmospheric pressure. The sliding generally involves plastic flow and surface cracking in silicon carbide. Figure 8 shows scanning electron micrographs of the wear track and wear debris generated during sliding process of rider on the silicon carbide {0001} surface. In Fig. 8(a), both the loading and tangential force were applied to the specimen, but no gross sliding of rider was observed.

A sector-shaped light area adjacent to and ahead of wear track (plastic identation) made by rider is a large particle of wear debris which was generated by both tangential and normal forces during microsliding of the rider. A large number of small wear debris particles are also generated during loading and microsliding by rider. It is anticipated from Fig. 8(a) that gross fracturing is primarily due to cleavage-cracking along $\{10\bar{1}0\}$ planes and subsurface-cleavage-cracking made by microsliding of the rider. Further, Fig. 8(b) shows a scanning electron micrograph of wear track and wear debris after gross sliding.

Figure 8(b) reveals the wear debris has been divided (fractured) by gross-sliding of rider, and the wear track is plastically deformed. The gross wear debris has sharp edges generated by cleavage cracking of $\{10\bar{1}0\}$ planes. At the third stage of the fracturing process, the gross wear debris particles fractured, divided and was ejected from the wear track. The track, where the wear debris particle was ejected reveals that the fracturing is the result of surface cracking. This is a result of cleavage of the $\{10\bar{1}0\}$ planes and subsurface cracking occurring with cleavage along {0001}

planes. Figure 9 reveals the wear tracks accompanied by fracture. Again, this is primarily due to surface cracking of $\{10\bar{1}0\}$ planes observed on both sides of the wear track and subsurface cracking of $\{0001\}$ planes. The wear debris particles were ejected from the wear track.

Thus, the fracture behavior of silicon carbide during sliding, as mentioned above, may be explained in terms of the fracture energy acting in the $\{10\bar{1}0\}$ cleavage system (primary cracking system) during slidings in the $\langle 10\bar{1}0\rangle$ and $\langle 11\bar{2}0\rangle$ directions on a (0001) silicon carbide surface.

Figure 10 shows typical scanning electron micrographs of the grooves on the silicon carbide $\{10\bar{1}0\}$ and $\{11\bar{2}0\}$ surfaces generated by a single pass of the diamond rider. In Fig. 10, the rectangular area consists of a large crack with lodged wear debris, where the cracks were generated, propagated, and then intersected during sliding of the rider. The cracking generally depends on the crystallographic orientation. The surface cracks propagate primarily in the $\langle 0001\rangle$ and $\langle 11\bar{2}0\rangle$ or $\langle 10\bar{1}0\rangle$ directions. The formations of these cracks are due to the surface-cleavage cracking along the $\{0001\}$ and $\{11\bar{2}0\}$ or $\{10\bar{1}0\}$ planes, respectively. It is anticipated from Figs. 8 and 9 that subsurface cracking also occurs underneath the lodged rectangular wear debris.

Figure 11 reveals a gross fracture pit where the gross wear debris particle has already been ejected. The fracture pit reveals that the fracturing is the result of surface cracking along primary cleavage planes $\{10\bar{1}0\}$ and $\{0001\}$ and subsurface cracking along $\{10\bar{1}0\}$, as anticipated. In the Fig. 11 sharp edges zig-zag along the $\{10\bar{1}0\}$ and $\{0001\}$ cleavage planes. The bottom surface of the fracture pit is parallel to the sliding surface.

Thus, again the fracture of silicon carbide during sliding on the $\{10\bar{1}0\}$ and $\{11\bar{2}0\}$ surfaces in various directions (such as $\langle 0001\rangle$, $\langle 10\bar{1}0\rangle$, or $\langle 11\bar{2}0\rangle$) is explained in terms of the fracture energy acting in the $\{10\bar{1}0\}$, $\{11\bar{2}0\}$, and $\{0001\}$ cleavage systems.

Friction. The coefficient of friction and width of the permanent grooves, involving plastic flow and surface cracking, were measured as functions of the crystallographic direction of sliding on the $\{0001\}$, $\{10\bar{1}0\}$, and $\{11\bar{2}0\}$ planes of silicon carbide for the diamond rider in mineral oil. The widths of the permanent grooves were obtained by average measurements of 20 samples from 7 to 10 scanning electron micrographs. The results presented in Fig. 12 indicate that the coefficient of friction and the groove width are influenced by the crystallographic orientation. The $\langle 11\bar{2}0\rangle$ direction on the basal $\{0001\}$ plane has the larger groove, primarily resulting from plastic flow and is the direction of high friction for this plane. The $\langle 0001\rangle$ directions on the $\{10\bar{1}0\}$ and $\{11\bar{2}0\}$ planes have the greater groove width and are the directions of high friction when compared with $\langle 11\bar{2}0\rangle$ on $\{10\bar{1}0\}$ and $\langle 10\bar{1}0\rangle$ on the $\{11\bar{2}0\}$ planes. The anisotropies of friction are $\mu\langle 11\bar{2}0\rangle/\mu\langle 10\bar{1}0\rangle = 1.2$ on $\{0001\}$, $\mu\langle 0001\rangle/\mu\langle 11\bar{2}0\rangle = 1.3$ on $\{10\bar{1}0\}$, and $\mu\langle 0001\rangle/\mu\langle 10\bar{1}0\rangle = 1.3$ on $\{11\bar{2}0\}$.

Figure 12 also represents the contact pressure calculated from the data of the groove width in Fig. 12(b) and the Knoop hardness obtained by Shaffer (26). The anisotropies of the contact pressure during sliding and the Knoop hardness clearly correlate with each other.

Several slip systems have been observed in hexagonal silicon carbide, such as $\{0001\}\langle 11\bar{2}0\rangle$, $\{3301\}\langle 11\bar{2}0\rangle$, and $\{10\bar{1}0\}\langle 11\bar{2}0\rangle$ (24,25). The $\{10\bar{1}0\}\langle 11\bar{2}0\rangle$ slip system observed on the sliding surface was responsible for the anisotropic friction and deformation behavior of silicon carbide during sliding in the $\langle 10\bar{1}0\rangle$ and $\langle 11\bar{2}0\rangle$ directions on a $\{0001\}$ silicon carbide surface. The experimental results on the $\{0001\}$ plane generally agreed with Daniel and Dunn's (28) resolved shear stress analysis based on the slip system $\{10\bar{1}0\}\langle 11\bar{2}0\rangle$. The minimum and maxima of the resolved shear stress for the $\{0001\}$ plane of hexagonal crystal match the hard and soft directions on that plane, that is, the $\langle 10\bar{1}0\rangle$ and $\langle 11\bar{2}0\rangle$ directions, respectively. These experimental results can not be explained by the Brookes, O'Neill, and Redfern's (25) resolved shear stress analysis based on the $\{0001\}\langle 11\bar{2}0\rangle$ slip system. Thus, the anisotropies of friction and hardness on the $\{0001\}$ plane strongly correlate with the resolved shear stress, based on the slip system $\{10\bar{1}0\}\langle 11\bar{2}0\rangle$.

The anisotropies of friction, contact pressure (groove width), and Knoop hardness on the $\{10\bar{1}0\}$ and $\{11\bar{2}0\}$ planes were correlated with Ref. 28's resolved shear stress based on the $\{10\bar{1}0\}\langle 0001\rangle$ and $\{10\bar{1}0\}\langle 11\bar{2}0\rangle$ slip systems. They were also correlated with Ref. 25's resolved shear stress based on the $\{\bar{1}210\}\langle 10\bar{1}0\rangle$ slip system. However, the slip system actually observed in hexagonal silicon carbide, the $\{10\bar{1}0\}\langle 11\bar{2}0\rangle$ slip system, may be responsible for those anisotropies on the $\{10\bar{1}0\}$ and $\{11\bar{2}0\}$ planes.

Similar data for Knoop hardness anisotropy of tungsten carbide $\{0001\}$ and $\{10\bar{1}0\}$ surfaces have been reported by French and Thomas (29) who used a resolved shear-stress calculation involving the $\{10\bar{1}0\}\langle 0001\rangle$ and $\{10\bar{1}0\}\langle 11\bar{2}0\rangle$ slip systems to explain the data. Thus, the anisotropies of friction, contact pressure, and Knoop hardness on the $\{0001\}$, $\{10\bar{1}0\}$, and $\{11\bar{2}0\}$ planes of silicon carbide are primarily controlled by the slip system $\{10\bar{1}0\}\langle 11\bar{2}0\rangle$.

Figure 12 suggest that the $\langle 10\bar{1}0\rangle$ on the basal plane of silicon carbide would exhibit the lowest coefficient of friction and greatest resistance to abrasion resulting from plastic deformation.

CONCLUSIONS

The following conclusions are drawn from this study of silicon carbide surfaces after sliding contact with diamond, metals or itself.

Adhesive Friction and Wear

1. Hexagon-shaped pits of silicon carbide and the formation of platelet multiangular wear debris, including hexagon-shaped wear debris, are observed as a result of sliding of single-crystal silicon carbide against metals and itself. The formation of pits and wear debris is due to cleavage of $\{0001\}$, $\{10\bar{1}0\}$ and $\{11\bar{2}0\}$ planes.

2. The coefficient of friction is markedly dependent on the orientation and it is lower in the $\langle 11\bar{2}0\rangle$ direction than that in the $\langle 10\bar{1}0\rangle$ direction. That is the force resisting shearing fracture of the adhesive bonds at the interface is lower in preferred crystallographic direction of slip.

Abrasive Wear and Friction

1. The $\langle 10\bar{1}0\rangle$ direction on the basal $\{0001\}$ plane of silicon carbide exhibits the lowest coefficient of friction and the greatest resistance to abrasion.

2. The anisotropic fracture during sliding on the basal plane is due to surface cracking along $\{10\bar{1}0\}$ and subsurface cracking along $\{0001\}$. The fracture during sliding on the $\{10\bar{1}0\}$ and $\{11\bar{2}0\}$ surfaces is due to surface cracking along $\{0001\}$ and $\{11\bar{2}0\}$ or $\{10\bar{1}0\}$ and to subsurface cracking along $\{10\bar{1}0\}$.

3. Anisotropic friction and deformation on the $\{0001\}$, $\{10\bar{1}0\}$, and $\{11\bar{2}0\}$ silicon carbide surfaces are primarily controlled by the slip system $\{10\bar{1}0\}\langle 11\bar{2}0\rangle$.

REFERENCES

1 O'Connor, J. R. and Smiltens, J., eds., Silicon Carbide, a High Temperature Semiconductor. Pergamon Press, New York, 1960.

2 Marshall, R. C., Faust, J. W., Jr., and Ryan, C. E., eds., Silicon Carbide - 1973; Proceedings of the Third International Conference. University of South Carolina Press, Columbia, 1974.

3 Miyoshi, K. and Buckley, D. H., "Friction and Wear Behavior of Single-Crystal Silicon Carbide in Sliding Contact with Various Metals," ASLE Transactions, Vol. 22, No. 3, 1979, pp. 245-256.

4 Miyoshi, K. and Buckley, D. H., "Adhesion, Friction, and Wear of Binary Alloys in Contact with Single-Crystal Silicon Carbide," NASA TM-79282, 1980.

5 Miyoshi, K. and Buckley, D. H., "The Friction and Wear of Metals and Binary Alloys in Contact with An Abrasive Grit of Single-Crystal Silicon Carbide," NASA TM-79131, 1979.

6 Bowden, F. P., Brooks, C. A., and Hanwell, A. E., "Anisotropy of Friction in Crystals," Nature, Vol. 203, No. 4940, 1964, pp. 27-30.

7 Buckley, D. H., "Influence of Orientation of Grains in Tungsten on Its Friction Characteristics," NASA TN-D-3238, 1966.

8 Steijn, R. P., "On the Wear of Sapphire," Journal of Applied Physics, Vol. 32, No. 10, Oct. 1961, pp. 1951-1958.

9 Duwell, E. J., "Friction and Wear of Single-Crystal Sapphire Sliding on Steel," Journal of Applied Physics, Vol. 33, No. 9, Sep. 1962, pp. 2691-2698.

10 Bowden, F. P. and Hanwell, A. E., "The Friction of Clean Crystal Surfaces," Proceedings of the Royal Society, London, Series A, Vol. 295, No. 1422, Dec. 1966, pp. 233-243.

11 Brown, W. R., Eiss, N. S., Jr., and McAdams, H. T., "Chemical Mechanism Contributing to Wear of Single-Crystal Sapphire on Steel," American Ceramic Society Journal, Vol. 47, No. 4, 1964, pp. 157-162.

12 Bowden, F. P. and Hanwell, A. E., "Friction and Wear of Diamond in High Vacuum," Nature, Vol. 201, No. 4926, 1964, pp. 1279-1281.

13 Seal, M., "The Abrasion of Diamond," Proceedings of the Royal Society, London, Series A, Vol. 248, No. 1254, Nov. 1958, pp. 379-393.

14 Bowden, F. P. and Brookes, C. A., "Frictional Anisotropy in Nonmetallic Crystals," Proceedings of the Royal Society, London, Series A, Vol. 295, No. 1442, Dec. 1966, pp. 244-258.

15 Tanaka, K., Miyoshi, K., and Miyao, Y., "Friction and Deformation of Mn-Zn Ferrite Single Crystals," Proceedings of the JSLE/ASLE International Lubrication Conference, T. Sakurai, ed., Elsevier Scientific Publishing Co., New York, 1976, pp. 58-66.

16 Miyoshi, K. and Buckley, D. H., "Friction and Wear of Single-Crystal Manganese-Zinc Ferrite," Wear of Materials, 1979, K. C. Ludema, W. A. Glaeser, and S. K. Rhee, eds., American Society of Mechanical Engineers, New York, 1979, pp. 509-519. Also NASA TM-78980, 1979.

17 Taylor, A. and Laidler, D. S., "The Formation and Crystal Structure of Silicon Carbide," British Journal Applied Physics, Vol. 1, 1950, pp. 174-181.

18 Hume-Rothery, W. and Raynor, G. V. The Structure of Metals and Alloys, 4th ed. rev., The Institute of Metals, Belgrave Square, London, S. W. 1, 1962.

19 Hasselman, D. P. H. and Batha, H. D., "Strength of Single Crystal Silicon Carbide," Applied Physics Letters, Vol. 2, No. 6, Mar. 15, 1963, pp. 111-113.

20 Bhagavantam, S. and Bhimasenachar, J., "Elastic Constants of Diamond," Proceedings of the Royal Society, London, Series A., Vol. 187, No. 1010, Nov. 5, 1946, pp. 381-384.

21 Miyoshi, K. and Buckley, D. H., "Anisotropic Friction, Deformation, and Fracture of Single-Crystal Silicon Carbide at Room Temperature," NASA TP-1525, 1979.

22 Van Bommel, A. J., Crombeen, J. E., and Van Tooren, A., "LEED and Auger Electron Observations of the SiC (0001) Surface," Surface Science, Vol. 48, 1975, pp. 463-472.

23 Miyoshi, K. and Buckley, D. H., "Wear Particles of Single-Crystal Silicon Carbide in Vacuum," NASA TP-1624, 1980.

24 Amelinckx, S., Strumane, G., and Webb, W. W., "Dislocations in Silicon Carbide," Journal of Applied Physics, Vol. 31, No. 8, Aug. 1960, pp. 1359-1370.

25 Brookes, C. A., O'Neill, J. B., and Redfern, B. A. W., "Anisotropy in the Hardness of Single Crystals," Proceedings of the Royal Society, London, Series A., Vol. 322, No. 1548, Mar. 1971, pp. 73-88.

26 Shaffer, Peter T. B., "Effect of Crystal Orientation on Hardness of Silicon Carbide," Journal of the American Ceramic Society, Vol. 47, No. 9, Sep. 1964, p. 466.

27 Adewoye, O. O., et al., "Structural Studies of Surface Deformation in MgO, SiC, and Si_3N_4," Annual Technical Report 1 Oct. 1973-30 Sep. 1974, Cambridge Univ., England, 1974. (AD-A008993)

28 Daniels, F. W. and Dunn, C. G., "The Effect of Orientation on Knoop Hardness of Single Crystals of Zinc and Silicon Ferrite," Transactions of the American Society for Metals, Vol. 41, 1949, pp. 419-442.

29 French, D. N. and Thomas, D. A., "Hardness Anisotropy and Slip in WC Crystals," American Institute of Mining, Metallurgical and Petroleum Engineers, Transactions, Vol. 233, May 1965, pp. 950-952.

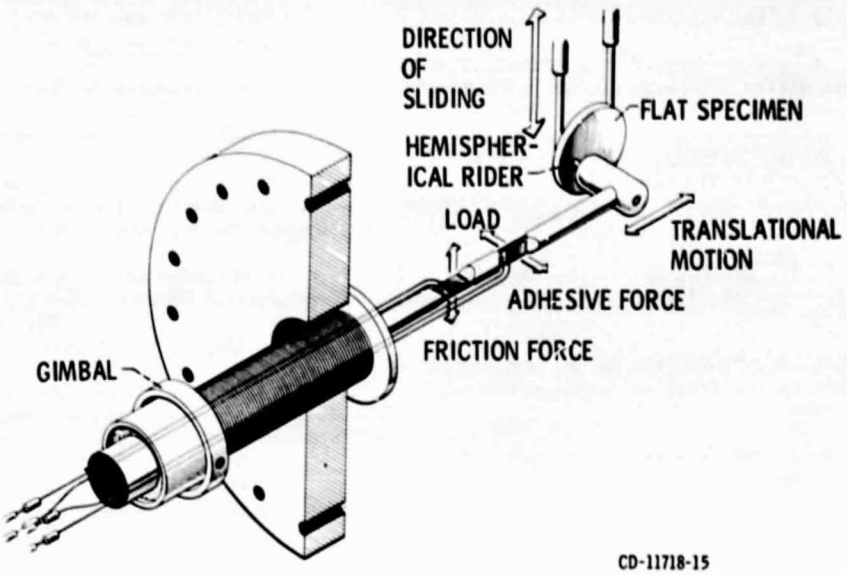

(a) High-vacuum apparatus.

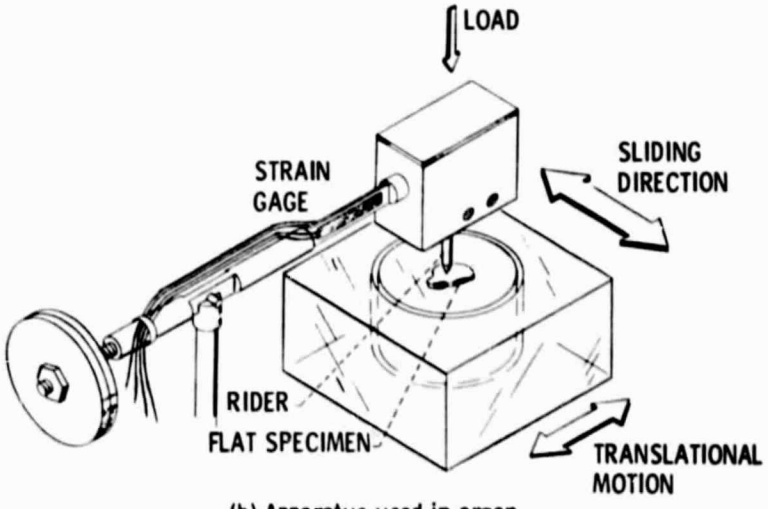

(b) Apparatus used in argon.

Figure 1. - Friction and wear apparatus.

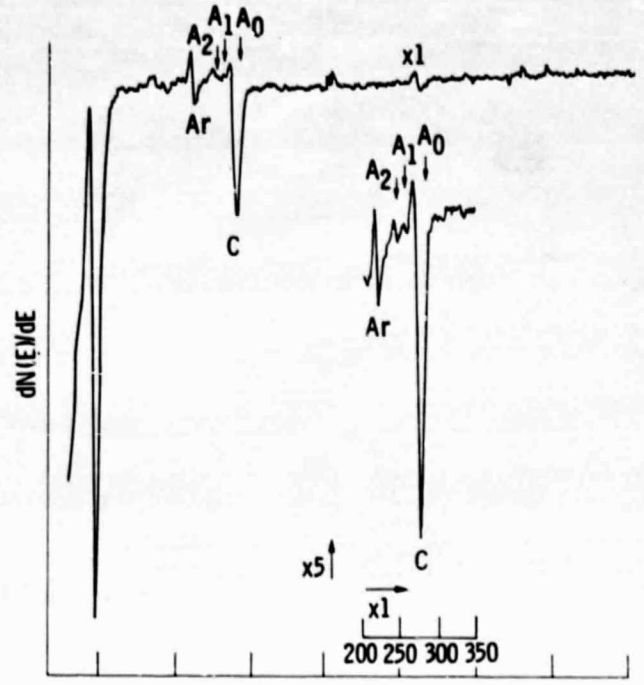

(a) Argon sputter cleaned surface.

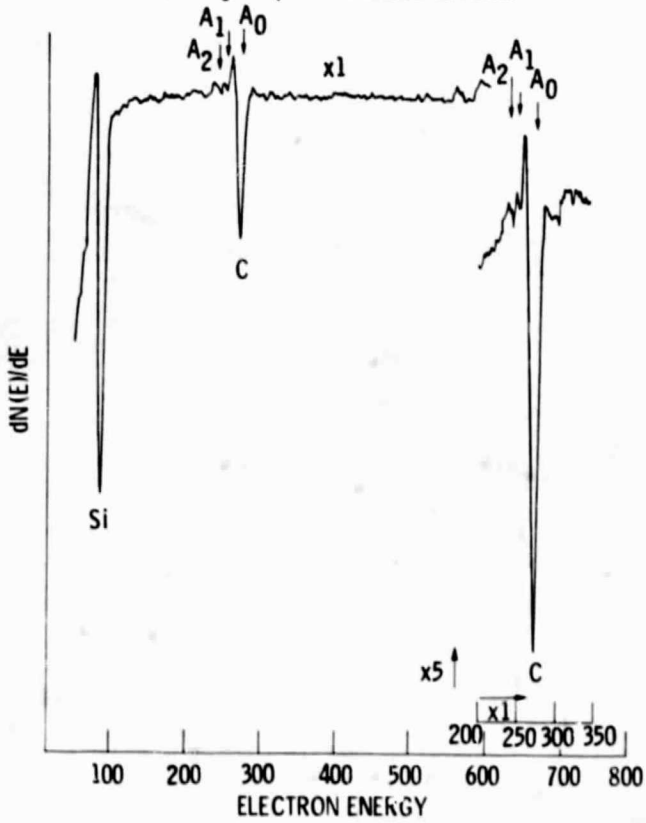

(b) Heat cleaned surface.

Figure 2. - Auger spectra of silicon carbide (0001) surface.

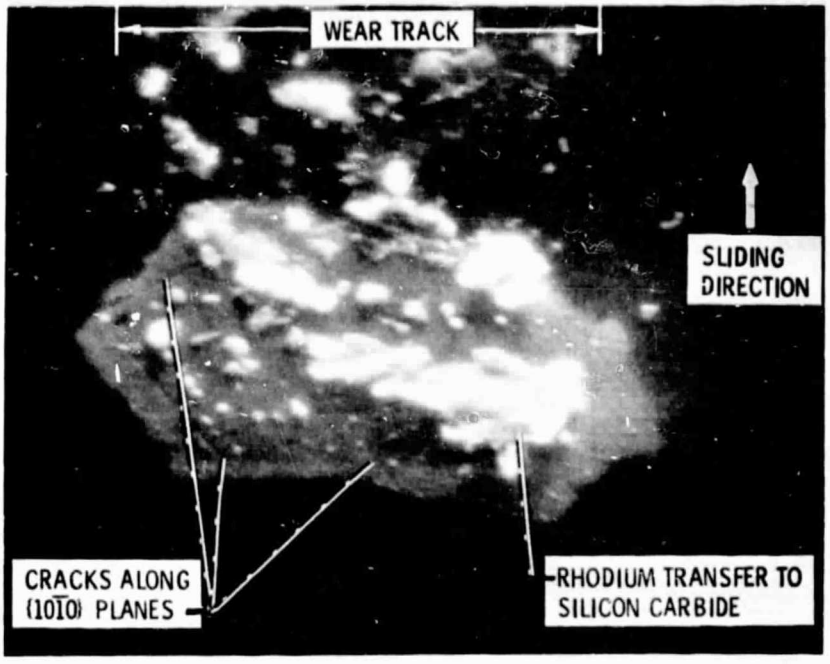

(a) HEXAGON-SHAPED CRACKING.

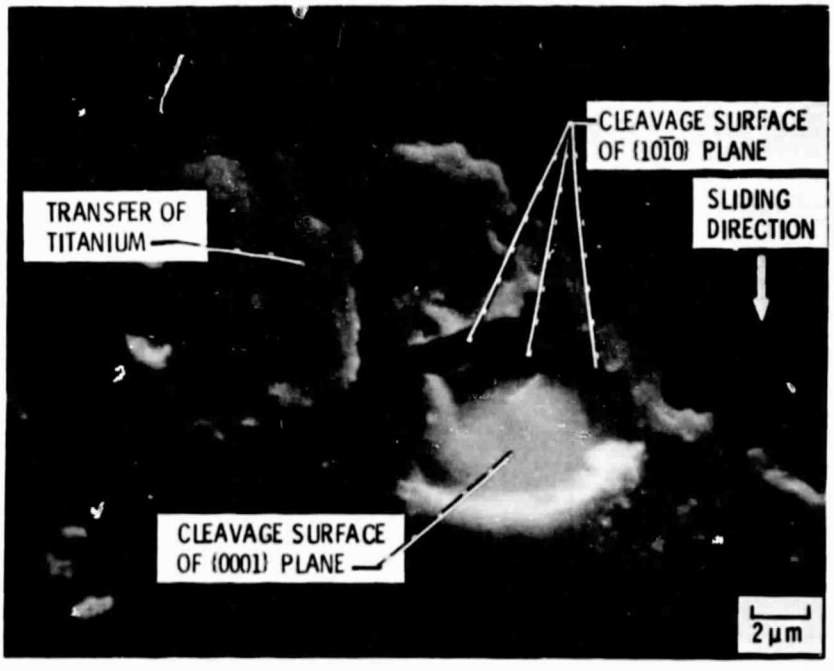

(b) HEXAGON-SHAPED PIT.

Figure 3. - Cracking and hexagon-shaped pit of single-crystal silicon carbide in contact with rhodium and titanium as result of 10 passes of rider in vacuum (10^{-8} Pa). Scanning electron micrographs of wear tracks on silicon carbide (0001) surface. Sliding direction, $\langle 10\bar{1}0 \rangle$; sliding velocity, 3 mm/min; load, 0.3 newton; room temperature.

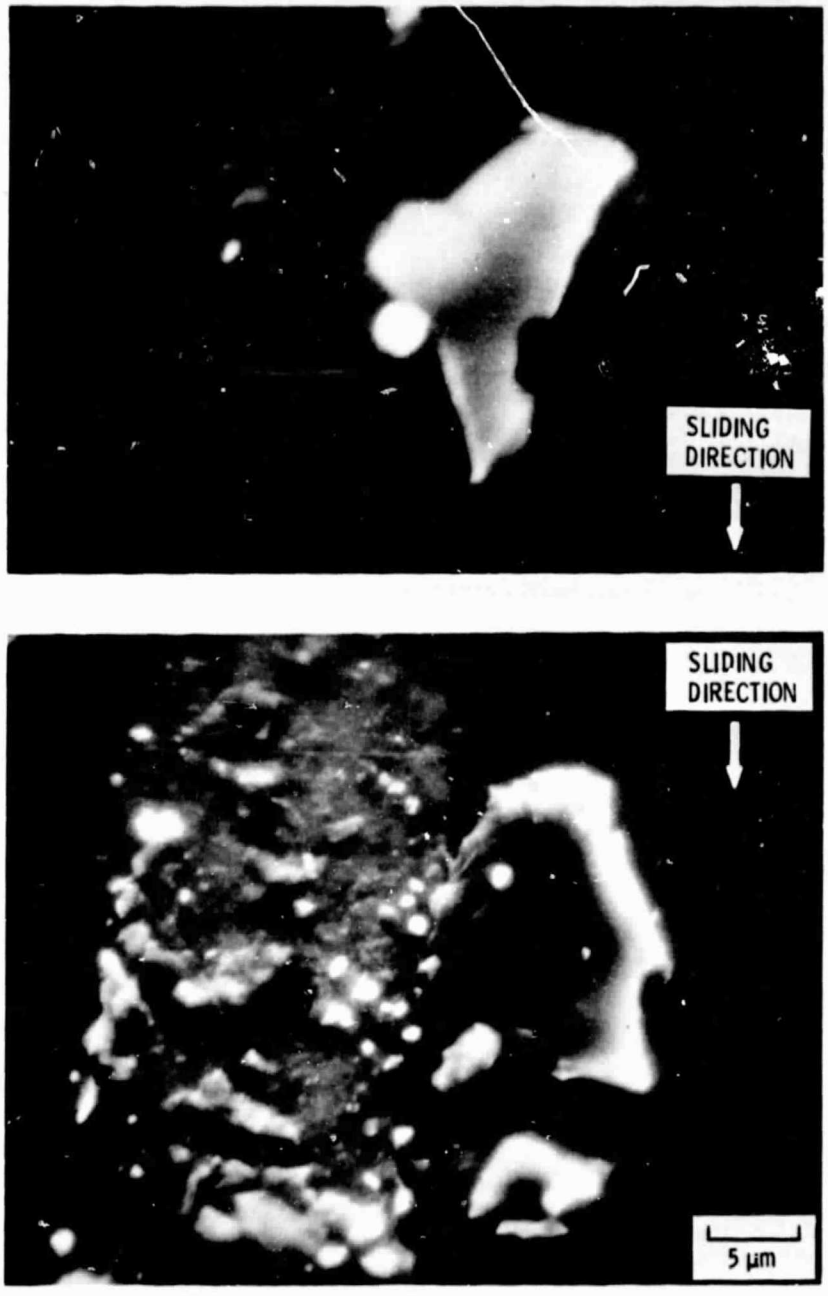

Figure 4. - Multiangular wear debris of single crystal silicon carbide as a result of 10 passes of aluminum riders in vacuum (10^{-8} Pa). Scanning electron micrographs of wear tracks on flat silicon carbide. Sliding velocity, 3×10^{-3} meter per minute; load, 0.2 newton, room temperature.

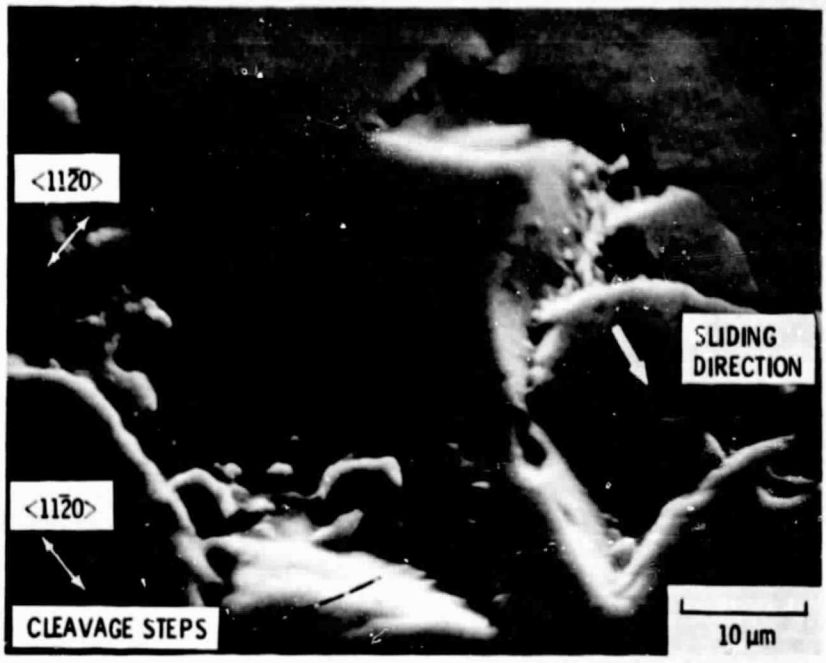

(a) HEXAGON-SHAPE FRACTURE.

(b) NEARLY COMPLETE HEXAGON-SHAPED WEAR DEBRIS.

Figure 5. - Hexagon-shaped fracture and wear debris of single-crystal silicon carbide in sliding contact with itself as a result of 10 passes of rider in vacuum. Sliding velocity, 3 mm/min; load, 0.5 N; room temperature, and 10^{-8} N/m^2.

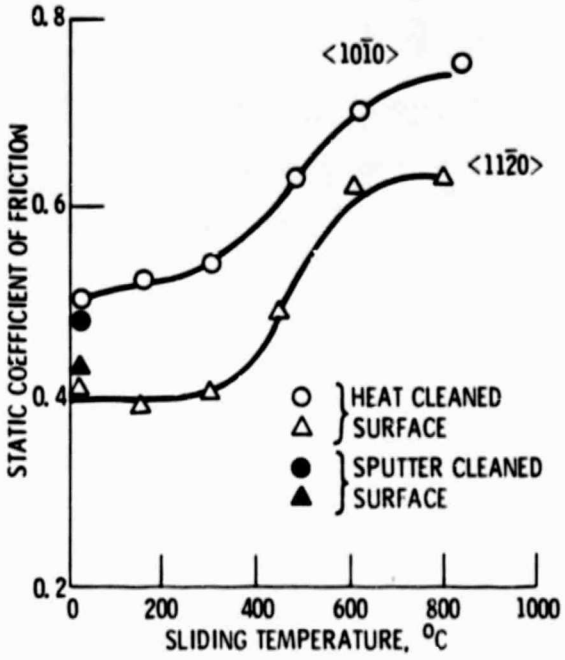

Figure 6. - Effect of temperature and crystallographic orientation of friction for silicon carbide (0001) surface sliding against iron rider. The silicon carbide surfaces were heat cleaned at 800° C before friction experiments. The coefficient of friction is obtained by averaging of 3 to 5 measurements Normal load, 0.2 N; vacuum, 10^{-8} Pa.

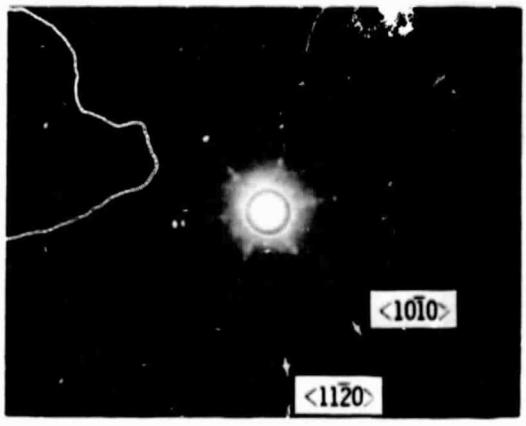

(a) BACK REFLECTION LAUE PHOTOGRAPH.

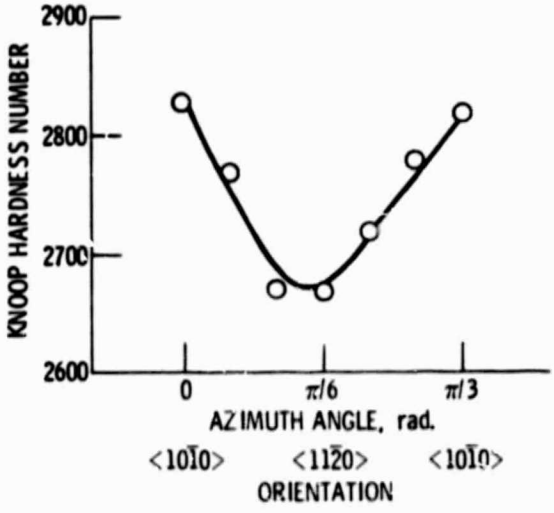

(b) KNOOP MICROHARDNESS ON THE {0001} BASAL PLANE OF SILICON CARBIDE AS A FUNCTION OF THE ANGLE BETWEEN THE LONG AXIS OF KNOOP INDENTER AND <10$\bar{1}$0> DIRECTION AXIS ON THE {0001} PLANE. MEASURING LOAD IS 2.9 N.

Figure 7. - Laue photograph and Knoop hardness of silicon carbide.

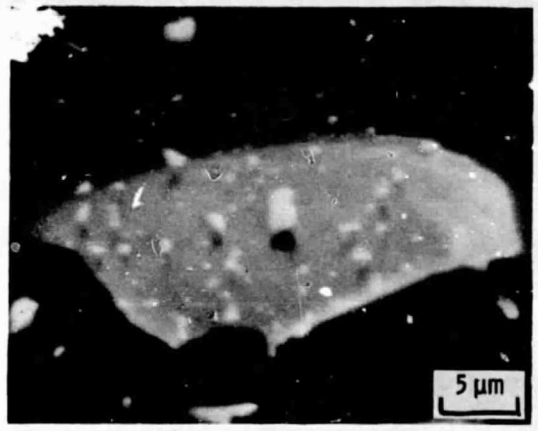

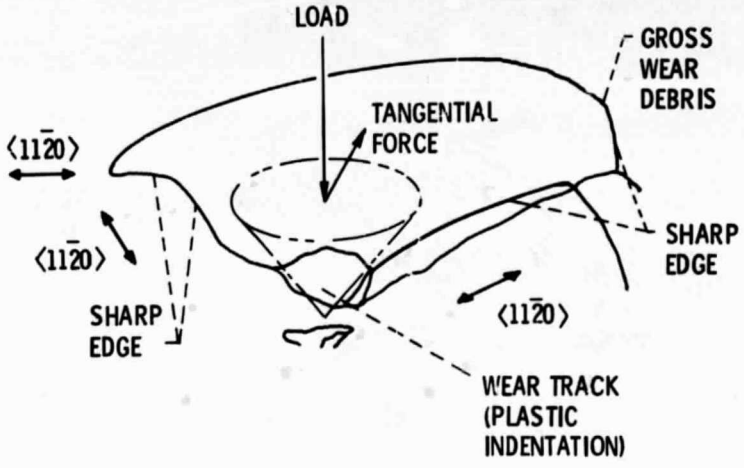

(a) FIRST STAGE (BEFORE GROSS SLIDING).

Figure 8. - Mechanism of fracture. Single pass of conical diamond rider; sliding surface (0001); sliding direction, <10$\bar{1}$0>; sliding velocity, 3 mm/min; load, 0.3 N; temperature, 25° C in argon at atmospheric pressure.

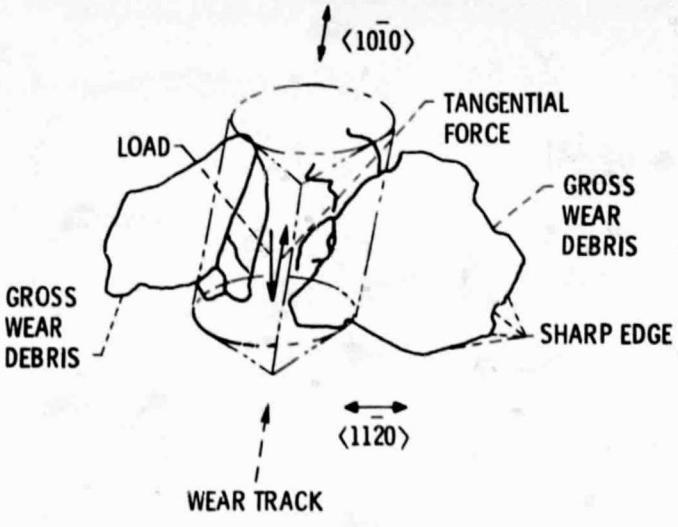

(b) SECOND STAGE (AFTER GROSS SLIDING).

Figure 8. - Concluded.

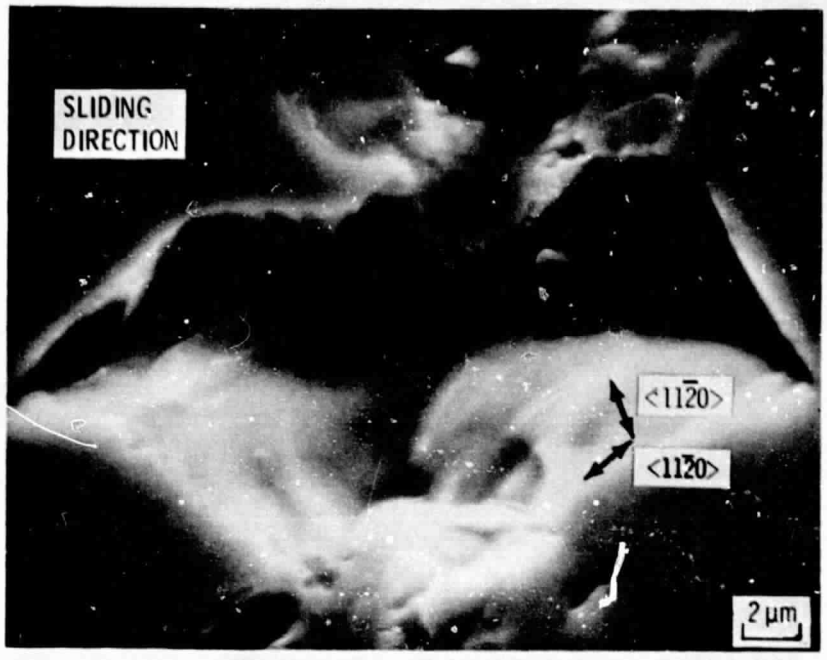

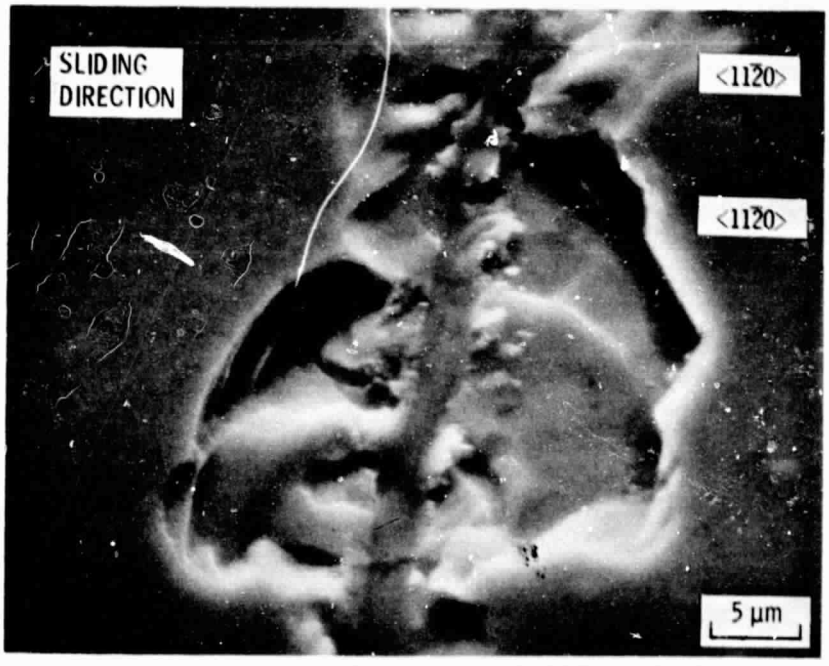

Figure 9. - Scanning electron micrographs of wear tracks accompanied with cleavage on a polished (0001) silicon carbide surface. Single pass of conical diamond rider; sliding direction, <10$\bar{1}$0>; sliding velocity, 3mm/min; load, 0.5 N; temperature, 25°C in argon at atmospheric pressure.

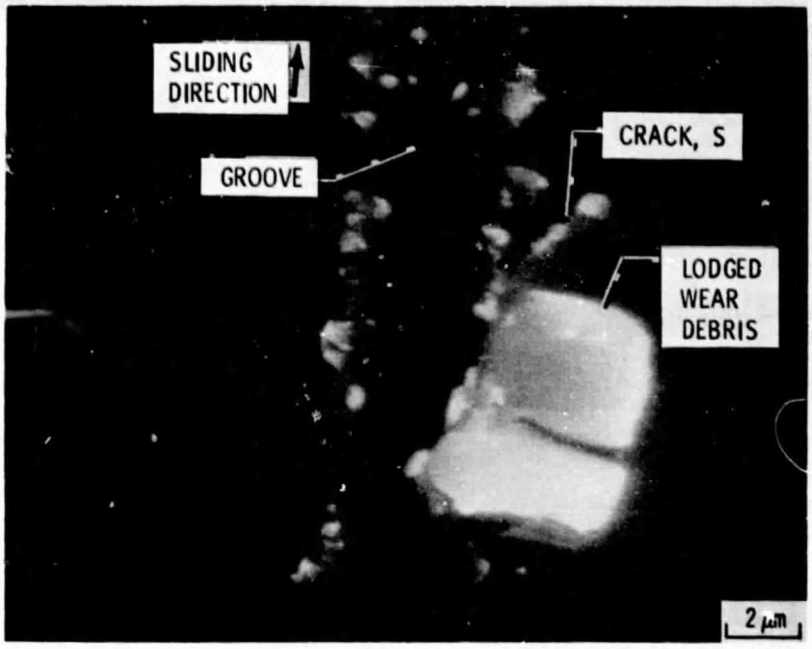

(a) AFTER SLIDING IN $\langle 11\bar{2}0 \rangle$ DIRECTION ON $\{10\bar{1}0\}$ PLANE.

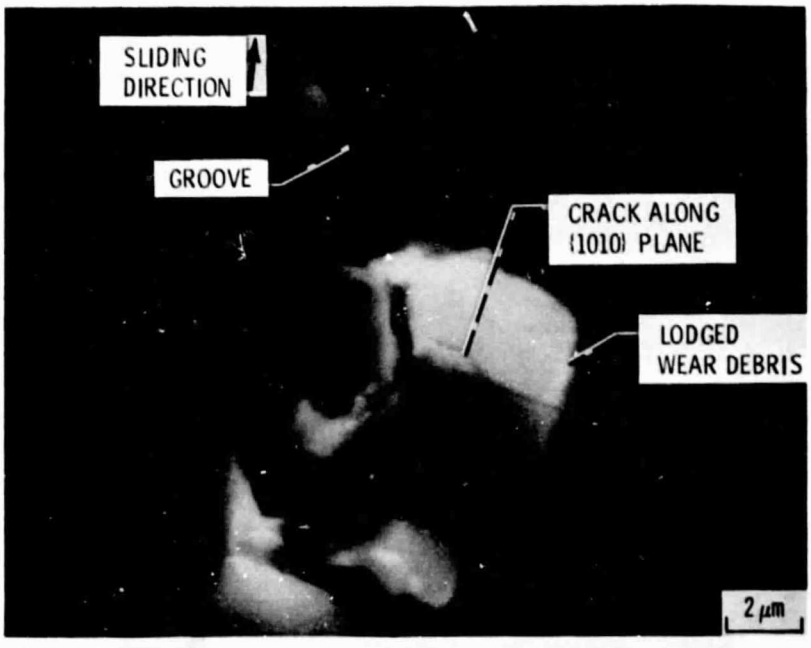

(b) AFTER SLIDING IN $\langle 10\bar{1}0 \rangle$ DIRECTION ON $\{11\bar{2}0\}$ PLANE.

Figure 10. - Scanning electron micrographs of grooves on $\{10\bar{1}0\}$ and $\{11\bar{2}0\}$ silicon carbide surfaces. Load, 0.2 N; in oil.

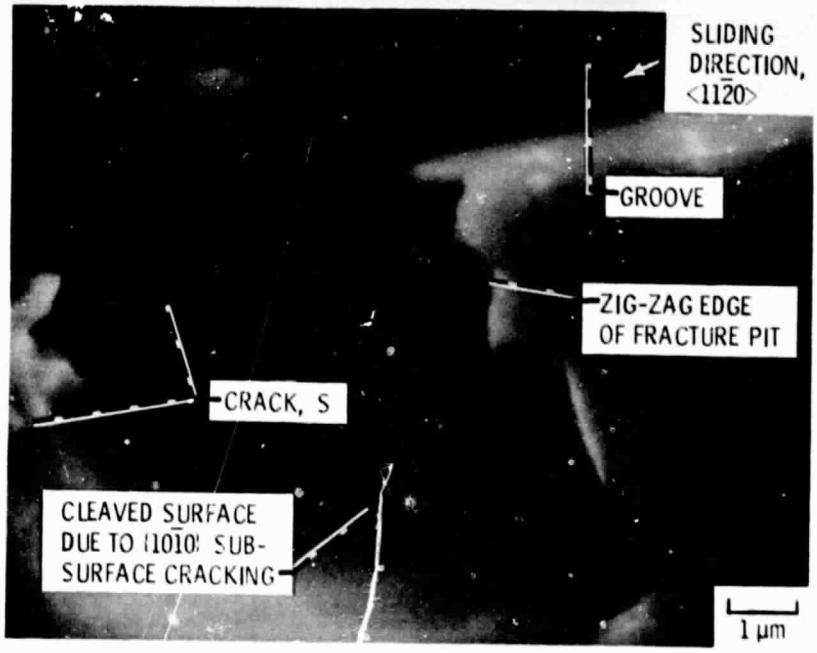

Figure 11. - Scanning electron micrograph of groove on $\{10\bar{1}0\}$ silicon carbide surface. Load, 0.2 N; in oil.

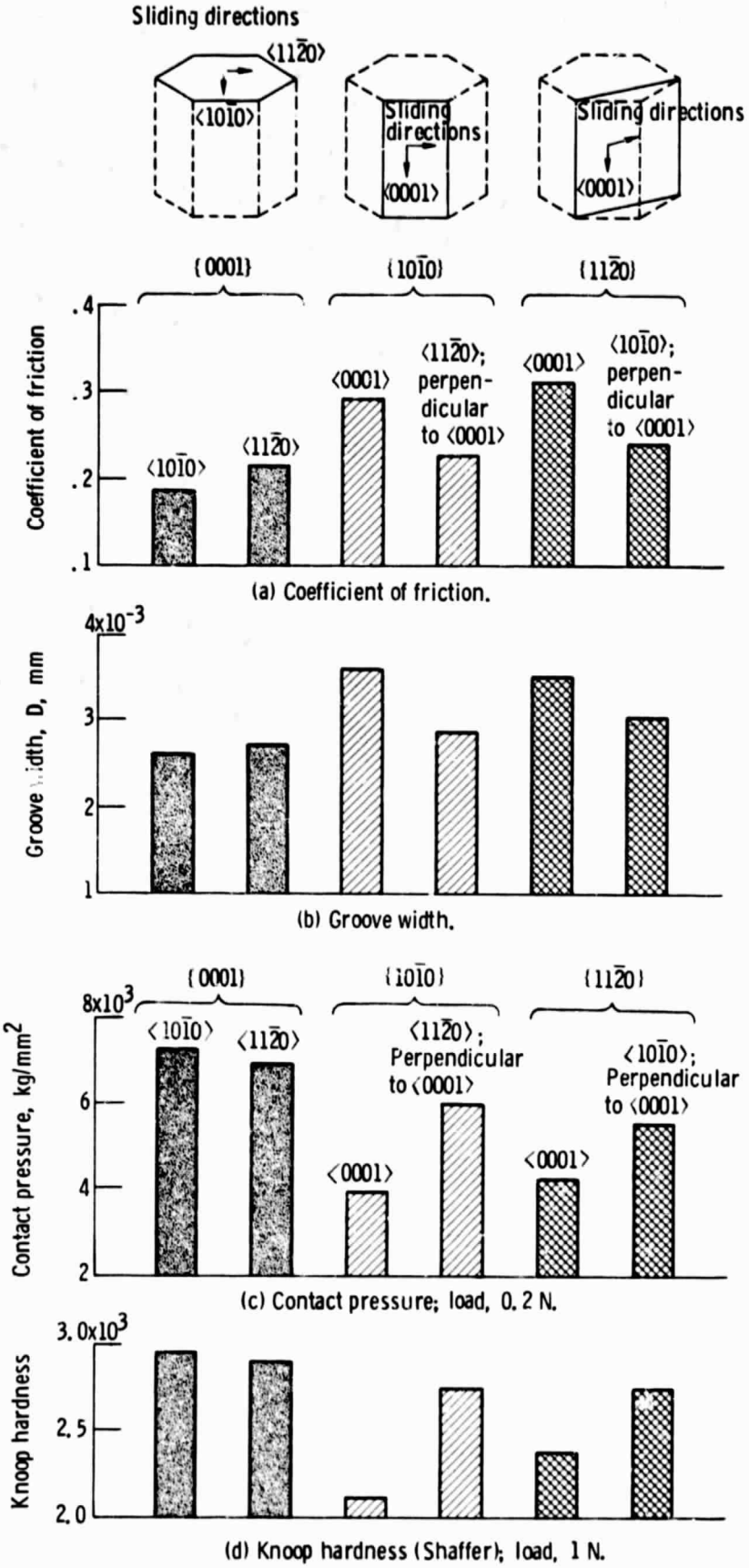

Figure 12. - Coefficients of friction, groove width, contact pressure, and Knoop hardness anisotropies on {0001}, {10$\bar{1}$0}, and {11$\bar{2}$0} silicon carbide surfaces.